

## Time-resolved pulsed-plasma characterization using broadband terahertz pulses correlated with fluorescence imaging

B. H. Kolner,<sup>a)</sup> P. M. Conklin, R. A. Buckles, N. K. Fontaine, and R. P. Scott  
*Department of Applied Science, University of California, Davis, One Shields Avenue,  
 Davis, California 95616*

(Received 17 May 2005; accepted 22 August 2005; published online 7 October 2005)

Near-monocycle terahertz (THz)-bandwidth electromagnetic pulses have been used to probe pulsed-discharge argon plasmas at various pressures from 10 to 50 Torr. Time-resolved electric field measurements were made of the THz pulse with and without plasma allowing a full characterization of the real and imaginary parts of the plasma index of refraction. Electron densities  $n_e \geq 10^{13} \text{ cm}^{-3}$  and collision rates  $\gamma_p \geq 10^{11} \text{ s}^{-1}$  were deduced by applying a simple Lorentz model to the measured time-domain pulse with no plasma and comparing it to the measured pulse with the plasma present. Minimizing the rms error between these in the two-dimensional parameter space  $(n_e, \gamma_p)$  fixed the values for each point in time of the plasma evolution. Optical fluorescence imaged transverse to the THz beam path was used to estimate the density profile used in the propagation model. © 2005 American Institute of Physics. [DOI: 10.1063/1.2103421]

The propagation of electromagnetic waves through a plasma for diagnostic purposes has inherent limitations, depending on the spectral region used and the source/detector technology.<sup>1</sup> For standard laboratory plasmas with electron densities in the range  $10^8 \text{ cm}^{-3} \leq n_e \leq 10^{14} \text{ cm}^{-3}$ , the plasma frequency lies in the range  $90 \text{ MHz} \leq f_p \leq 90 \text{ GHz}$ . Above this frequency the plasma is transparent and dispersive, below it is opaque. Probing the plasma at visible or near-infrared frequencies is typically so far above  $f_p$  that the plasma induces only a small phase shift and thus dynamic range is limited. Sources closer to  $f_p$ , such as molecular lasers and vacuum-tube devices, suffer from low power and limited tunability or, worse, are fixed in frequency. In a dynamically evolving plasma where the electron density changes dramatically, the plasma frequency might also rise above the probe frequency thus reflecting all of the power. Another issue with electromagnetic wave propagation-based diagnostics is that the wave acquires a net phase shift and attenuation due to the accumulated effect of the plasma which inevitably has a spatially varying density profile. For a given frequency,  $\omega$ , and density and collision rate profiles  $n_e(z)$  and  $\gamma_p(z)$ , respectively, the total phase shift acquired through a length  $L$  of plasma is

$$\phi(\omega, L) = \int_0^L \frac{\omega}{c} \sqrt{1 - \frac{n_e(z)e^2}{\epsilon_0 m[\omega^2 + i\omega\gamma_p(z)]}} dz. \quad (1)$$

Without prior knowledge of the shapes of the density and collision rate profiles, recovery of the absolute values of  $n_e(z)$  and  $\gamma_p(z)$  is difficult, at best. Finally, when continuous-wave sources are used to probe a plasma, the time resolution depends on the characteristics of the detector while for pulsed sources it is the source pulse width. The necessary performance of conventional sources and detectors is seldom available in the far-infrared and millimeter-wave portion of the spectrum, especially over large frequency ranges.

A nearly ideal source that overcomes most of these limitations is a terahertz (THz) pulse produced by a femtosecond

laser using either optical rectification<sup>2</sup> or photoconductive generation.<sup>3</sup> The short pulse duration allows time resolving plasma characteristics while the large frequency span encompasses a large range of density fluctuations. Recent work has demonstrated the efficacy of this approach but relied on approximating the plasma as having uniform spatial properties along the length of the THz beam.<sup>4,5</sup> Since the spatial distribution of plasma is seldom uniform, this approximation seriously limits accurate estimates of the peak density and collision rate. In this letter, we present a new technique which overcomes this limitation by applying a separate measurement, based on imaging the plasma fluorescence, to spatially model the density and collision rate profiles. We then apply a frequency domain model to compare the predicted pulse evolution with our data, thereby establishing peak values of  $n_e(z)$  and  $\gamma_p(z)$ .

Our terahertz time-domain spectroscopy (THz-TDS) system uses a GaAs photoconductive switch for pulse generation and a ZnTe crystal for electro-optic detection of the THz field-induced birefringence (Fig. 1). The photoconductive switch was fabricated on high-resistivity GaAs with photolithographically patterned gold-on-chrome electrodes bonded to copper blocks with silver paint.<sup>6</sup> These blocks serve both as terminals for a 100 V dc bias supply as well as heat sinks. The GaAs generation switch is illuminated with 30 fs pulses from a 100 MHz Ti:sapphire oscillator ( $\lambda = 800 \text{ nm}$ ) with a fluence of  $\approx 6 \mu\text{J}/\text{cm}^2$ . The Ti:sapphire beam is chopped at 600 Hz with an acousto-optic modulator for synchronous detection. Photoconductively generated THz pulses pass through the wafer and are collected with a 9.5 mm diameter silicon ball lens with its flat surface optically contacted to the wafer backside. This forms a waist 3 mm in front of the ball lens beyond which the beam diverges at a full angle of  $10^\circ$ . It is then focused into a vacuum chamber through a 15.9-mm-thick teflon window by an off-axis ellipsoidal mirror which produces a waist  $\approx 2 \text{ mm}$  in diameter in the center of the chamber. A second ellipsoidal mirror then refocuses the THz beam onto a ZnTe detection crystal where 25 mW of the Ti:sapphire beam samples the induced birefringence. The receiver is a standard electro-

<sup>a)</sup>Electronic mail: bhkolner@ucdavis.edu

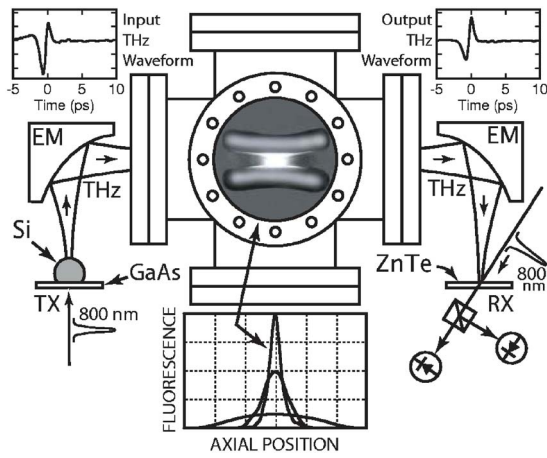


FIG. 1. Schematic diagram of experimental setup. THz transmitter (TX) uses GaAs photoconductive switch to generate 1 ps monocycle THz pulses which are collected by a silicon ball lens (Si) and focused by off-axis ellipsoidal mirrors (EM) into the vacuum chamber. Imaging of plasma fluorescence through viewport provides a good estimate of axial plasma density (shown in lower inset for 10, 30, and 50 Torr). Receiver (RX) uses electrooptic sampling in ZnTe to measure the THz electric field. Insets in upper-left and upper-right show THz measured wave form without plasma (input) and with plasma (output).

optic sampling arrangement with a quarter-wave plate and balanced photodiodes. The photodiode signals are sent to the boxcar integrator and then to a lockin amplifier which synchronously detects the 600 Hz modulation. The temporal resolution of the field measurement is  $<100$  fs.

Within the vacuum chamber are a pair of cylindrical electrodes, 12 mm in diameter, 75 mm long, and separated by 6 mm with their axes parallel to the THz beam. They are bent slightly to produce the highest electric field in the center of the chamber at the focus of the THz beam. A 1.5 kV, 10 ns pulse is delivered to the electrodes at a 10 kHz rate to ionize the gas. The longitudinal distribution of the plasma extends from several millimeters to over 75 mm in length and depends on the gas pressure. This strong dependence of spatial distribution on pressure suggested a separate measurement to improve evaluation of the integral in Eq. (1). For this we digitally image the transverse fluorescence through a glass viewport, take a line scan through the center of the image, and fit a smooth function to the scan which is then used as the  $z$ -dependent profile of  $n_e(z)$  and  $\gamma_p(z)$ .

Since the THz generation and sampling pulses run at 100 MHz and the plasma is pulsed at 10 kHz, a gated averager (boxcar integrator) is used to select a 60 ns window within the duration of the plasma. Thus, about six THz pulses sample the plasma every period of the 10 kHz high voltage pulse. The delay time of the boxcar window is incremented and at each step we measure the electric field of the THz pulse by scanning a mechanical delay stage in the excitation arm by  $\approx 40$  ps. Note: the 60 ns time window was chosen to obtain reasonable signal-to-noise ratio (SNR  $\approx 40$  dB). Each THz pulse is time resolved with  $<100$  fs resolution and we average six successive pulses to improve the SNR. (It is the absorption and phase shift measured in the THz pulse that provides the complex propagation characteristics of the plasma.) The net time resolution in terms of the plasma dynamics is therefore 60 ns which is deemed adequate for this experiment and allows us to probe a rather slowly evolving plasma with only a laser oscillator. The ul-

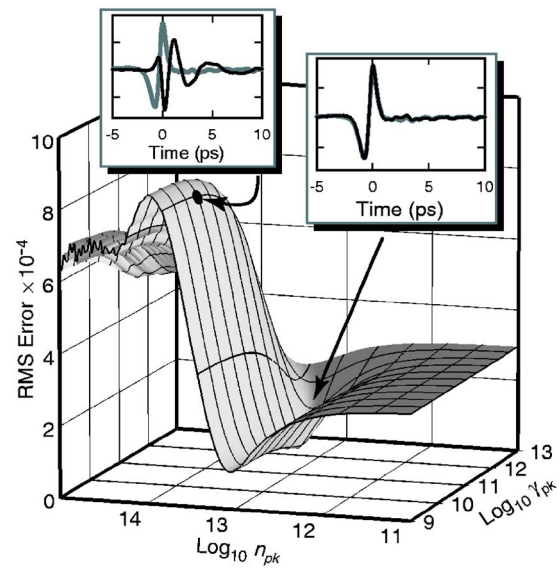


FIG. 2. rms error between measured THz pulse and that predicted using plasma phase shift in Eq. (1) with peak values of density and collision frequency ( $n_{pk}$ ,  $\gamma_{pk}$ ) as parameters. Insets show measured (light gray) and calculated wave form (black) at values of  $n_{pk}$  and  $\gamma_{pk}$  indicated by arrows. The time delay is 250 ns and the pressure is 30 Torr.

timate time resolution depends on the total time window. With higher power THz pulses, such as those produced by amplified fs laser pulses, only one pulse is needed to sample the plasma as in Ref. 4 and thus the resolution could be  $<40$  ps.

When the THz pulse passes through the plasma, each of the Fourier components in its spectral density function,  $\mathcal{E}(\omega)$ , obtains a phase shift  $\phi(\omega, L)$  according to Eq. (1). By superposition, the time-domain wave form is given by  $E(t, L) = \int_{-\infty}^{\infty} \mathcal{E}(\omega) \exp[i(\phi(\omega, L) - \omega t)] d\omega / 2\pi$ . In time-domain spectroscopy, we first measure a pulse that has propagated through the plasma and then one without the plasma (reference). Taking the ratio of their spectra establishes the complex transfer function for the propagation path:  $\mathcal{H}(\omega) \equiv \exp[i(\phi(\omega, L) - \omega L/c)]$ . Buried in this expression are integrals over the spatial profiles of  $n_e(z)$  and  $\gamma_p(z)$ . Finding  $\mathcal{H}(\omega)$  alone does not tell us much about these physical quantities. In order to establish the peak values of density and collision rate as well as a good approximation to their profiles, we employ a novel time-domain rms-error minimization technique that correlates the fluorescence profile and peak values of  $n_e(z)$  and  $\gamma_p(z)$  with measured time-domain wave forms. First, a reference pulse is Fourier transformed to the frequency domain where we apply the propagation transfer function  $\mathcal{H}(\omega)$ . We use Hermite-Gaussian functions to 20th order to curve fit the fluorescence line scans for  $n_e(z)$  and  $\gamma_p(z)$  in Eq. (1). The peak values,  $n_{pk}$  and  $\gamma_{pk}$  are set at the beginning of ranges that will be covered in repeated steps. The spectrum is then inverse Fourier-transformed and compared with the measured THz pulse that propagated through the plasma. We define an error function as the rms difference between these two wave forms and this value is saved in an array. The process is then repeated for a rectangular array of values of  $n_{pk}$  and  $\gamma_{pk}$ . A global minimum in this two-dimensional space indicates the best approximation to the peak values of density and collision rate. Figure 2 shows a plot of the two-dimensional surface of rms error versus  $n_{pk}$  and  $\gamma_{pk}$ . The insets show measured and calculated

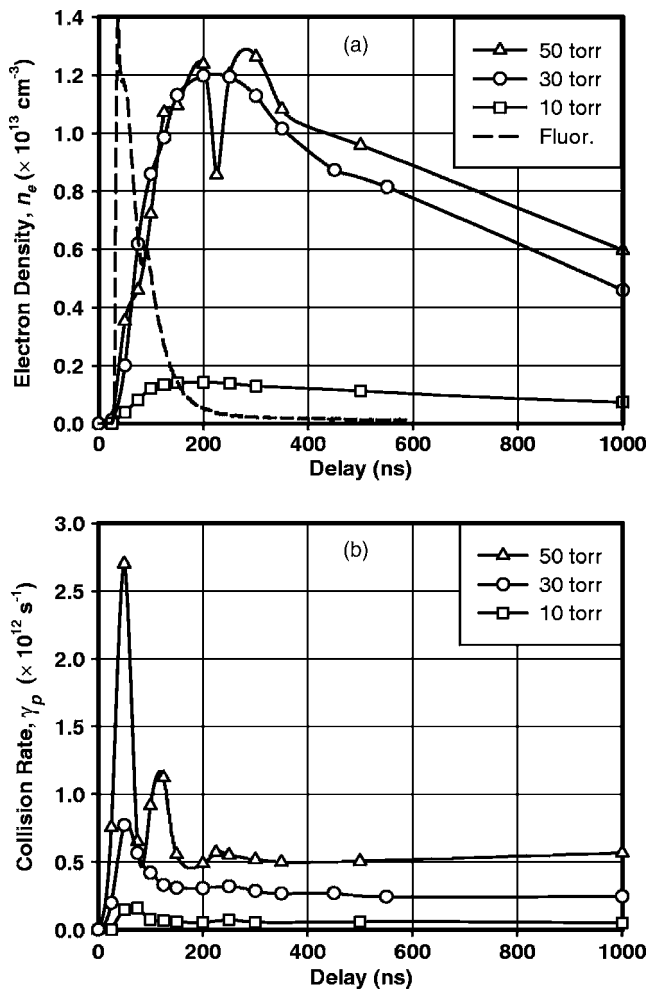


FIG. 3. (a) Pulsed argon plasma electron densities measured by THz-TDS for indicated pressures. Dashed curve is fluorescence brightness for 30 Torr measured with a high-speed photodiode. (b) Electron collision rate calculated from the same data.

THz time wave forms based on the values of  $n_{pk}$  and  $\gamma_{pk}$  at two points in the array. The close match at the global minimum demonstrates the effectiveness of this approach. Finally, this whole process is repeated for every time delay step of the boxcar (i.e., the time between the arrival of the gated THz pulses and the ignition of the plasma). In this way, a time profile of the variation in peak density and collision rate is obtained.

Figure 3 shows the results of these time-resolved density (a) and collision-rate (b) measurements for three different values of argon gas pressure (10, 30, and 50 Torr). Peak electron densities of  $n_e > 1 \times 10^{13} \text{ cm}^{-3}$  corresponding to a plasma frequency  $\omega_p \approx 2\pi \times 30 \text{ GHz}$  and collision rates  $\gamma_p > 2 \times 10^{12} \text{ s}^{-1}$  are measured with time resolution  $\delta t \approx 60 \text{ ns}$  (limited by the group of THz pulses used at each delay point). The apparently anomalous dip in the 50 Torr data is repeatable and may be caused by reflections on the transmission line between the pulsed high voltage supply and the time-varying impedance presented by the plasma.

The relationship between the electron density and the time-dependent fluorescence is complicated by the different mechanisms that could be involved (recombination, bound-bound transitions, free-free transitions (bremsstrahlung), etc.). The dashed line in Fig. 3(a) is a time record of the fluorescence emitted from the 30 Torr plasma measured with a high-speed photodiode indicating that the fluorescence has diminished to near-zero long before the plasma density has reached its peak. This suggests that the fluorescence is due mainly to the rapid radiative decay of highly excited argon atoms rather than recombination with the free electrons. (As such, we assume that both the electron density and the collision rate are spatially correlated with the fluorescence.)

During the high energy, nonequilibrium phase, secondary and tertiary ionization proceeds to build up the plasma density as the current pulse trails off. Eventually the electrons cool due to collisions and the density begins to fall as the plasma diffuses and recombines. From the peak densities at the indicated pressures we calculate an ionization fraction of  $\approx 10^{-5}$ . By about 200–300 ns, assuming local thermodynamic equilibrium, we can apply the Saha equation and estimate a peak electron temperature of  $T_e \approx 6 \times 10^3 \text{ K}$ .

In the early stages of the evolution of the plasma, the rapid rise in collision frequency [Fig. 3(a)] is due to the rapid generation of background ions which produce a much stronger effect due to long range Coulomb interaction<sup>7</sup> and is temporally correlated with the optical fluorescence. As the plasma heats and the density peaks, the collision frequency goes down because of the high electron velocity and thus lower cross section:  $\gamma_p \propto (kT_e)^{-3/2}$ . Later, the plasma cools and as the density is reduced, the collision frequency appears to level out on the time scale shown.

In summary we have introduced a powerful new tool for time-resolved plasma density and collision rate diagnostics using THz pulses correlated with imaging of the transverse fluorescence to estimate the spatial plasma profile.

*Note Added in Proof.* Another approach to extracting the propagation parameters from THz waveforms can be found in Ref. 8.

The authors wish to thank C. E. Hunt and N. Chubun for fabrication of the GaAs emitter and P. C. M. Planken for helpful discussions.

<sup>1</sup>M. A. Heald and C. B. Wharton, *Plasma Diagnostics with Microwaves* (Wiley, New York, 1965).

<sup>2</sup>D. H. Auston and K. P. Cheung, *J. Opt. Soc. Am. B* **2**, 606 (1985).

<sup>3</sup>X. Zhang, B. B. Hu, J. T. Darrow, and D. H. Auston, *Appl. Phys. Lett.* **56**, 1011 (1990).

<sup>4</sup>S. P. Jamison, J. Shen, D. R. Jones, R. C. Isaac, B. Ersfeld, and D. A. Jaroszynski, *J. Appl. Phys.* **93**, 4334 (2003).

<sup>5</sup>B. H. Kolner, P. M. Conklin, N. K. Fontaine, R. A. Buckles, and R. P. Scott, *Proceedings of the Optical Terahertz Science and Technology Conference*, Orlando, FL, Opt. Soc. America, 14–16 March 2005, Paper MD4.

<sup>6</sup>G. Zhao, R. N. Schouten, N. van der Valk, W. T. Wenckebach, and P. C. M. Planken, *Rev. Sci. Instrum.* **73**, 1715 (2002).

<sup>7</sup>F. F. Chen, *Introduction to Plasma Physics and Controlled Fusion*, 2nd ed. (Plenum, New York, 1984).

<sup>8</sup>L. DuVillaret, F. Garet, and J-L Coutaz, *IEEE J. Sel. Top. Quantum Electron.* **2**, 739 (1996).